

Isoscalar dipole transition as a probe for asymmetric clustering

Y. Chiba and M. Kimura*

Department of Physics, Hokkaido University, Sapporo 060-0810, Japan

Y. Taniguchi

Department of Medical and General Sciences, Nihon Institute of Medical Science, Moroyama, Saitama 350-0435, Japan

(Received 27 December 2015; published 17 March 2016)

Background: The sharp 1^- resonances with enhanced isoscalar dipole transition strengths are observed in many light nuclei at relatively small excitation energies, but their nature has been unclear.

Purpose: We show those resonances can be attributed to the cluster states with asymmetric configurations such as $\alpha + {}^{16}\text{O}$. We explain why asymmetric cluster states are strongly excited by the isoscalar dipole transition. We also provide a theoretical prediction of the isoscalar dipole transitions in ${}^{20}\text{Ne}$ and ${}^{44}\text{Ti}$.

Method: The transition matrix is analytically derived to clarify the excitation mechanism. The nuclear model calculations by Brink–Bloch wave function and antisymmetrized molecular dynamics are also performed to provide a theoretical prediction for ${}^{20}\text{Ne}$ and ${}^{44}\text{Ti}$.

Results: It is shown that the transition matrix is as large as the Weisskopf estimate even though the ground state is an ideal shell-model state. Furthermore, it is considerably amplified if the ground state has cluster correlation. The nuclear model calculations predict large transition matrix to the $\alpha + {}^{16}\text{O}$ and $\alpha + {}^{40}\text{Ca}$ cluster states comparable with or larger than the Weisskopf estimate.

Conclusions: We conclude that the asymmetric cluster states are strongly excited by the isoscalar dipole transition. Combined with the isoscalar monopole transition that populates the 0^+ cluster states, the isoscalar transitions are promising probes for asymmetric clusters.

DOI: [10.1103/PhysRevC.93.034319](https://doi.org/10.1103/PhysRevC.93.034319)

I. INTRODUCTION

The observed electric monopole ($E0$) and isoscalar (IS) monopole strength distributions of light nuclei [1–14] show that a considerable amount of the strength fractions appears at relatively small excitation energy as sharp resonances. It was known that many of those resonances are associated with the α cluster states such as the Hoyle state of ${}^{12}\text{C}$ [15–24], the $\alpha + {}^{12}\text{C}$ cluster states in ${}^{16}\text{O}$ [25,26], the $\alpha + {}^{16}\text{O}$ cluster states in ${}^{20}\text{Ne}$ [27], and the $\alpha + \alpha + t$ cluster state in ${}^{11}\text{B}$ [28–30]. Therefore, the IS monopole transition has been utilized as a probe to search for the cluster states in light nuclei. Later, Yamada *et al.* [31] clearly explained the enhancement mechanism of the monopole transition from the ground state to the cluster states. They showed, by exploiting the Bayman–Bohr theorem [32], that the degrees of freedom of cluster excitation are embedded in the ground state, and the monopole operator activates them to strongly excite the cluster states. This finding boosted the studies of the cluster states by using the monopole transition as a probe. In these days, various cluster states in stable and unstable nuclei [33–40] are discussed on the basis of their enhanced monopole strengths.

Among the various cluster states, the cluster systems with asymmetric configuration must have the 1^- state that constitute the parity doublet together with the 0^+ cluster state. For example, the 1^- state of ${}^{16}\text{O}$ at 9.6 MeV and that of ${}^{20}\text{Ne}$ at 5.8 MeV are the evidence of the asymmetric clustering with $\alpha + {}^{12}\text{C}$ and $\alpha + {}^{16}\text{O}$ configurations [41].

Therefore, identifying the 1^- cluster state is a key to prove asymmetric clustering. In the case of $N \neq Z$ nuclei, the enhanced electric-dipole ($E1$) transition was suggested as a probe for such 1^- states [42]. The 1^- cluster states with the $\alpha + {}^{14}\text{C}$ configuration in ${}^{18}\text{O}$ were experimentally searched by using the $E1$ strength as a probe [43,44], in addition to the ordinary experimental methods such as α scattering and breakup [45–48]. The α clustering in the actinides [49–51] were also investigated in the same literature. Recently, the α clustering in ${}^{212}\text{Po}$ [52–54] and the rare-earth nuclei [55] were also discussed based on their enhanced low-lying $E1$ strengths.

In the case of the $N = Z$ nuclei for which we expect a rich variety of clustering, the $E1$ transition is not available and we need other probes. As an alternative, one may consider the IS dipole transition, because it populates 1^- states and has an operator form that is similar to the IS monopole transition. Furthermore, its strength distributions measured for light nuclei [4–6,10,11,13,35,36] show the existence of the sharp resonances with enhanced strengths at relatively small excitation energies well below the giant resonance. In a recent experimental study [35], the observed low-lying resonances in ${}^{32}\text{S}$ are conjectured to be the $\alpha + {}^{28}\text{Si}$ cluster states, because of their enhanced IS dipole transition strength from the ground state. Very recently, Kanada–En’yo also discussed the enhancement of the IS dipole transition strength of the α cluster states in ${}^{12}\text{C}$ based on a theoretical calculation [56]. However, the excitation mechanism of the IS dipole transition and the relationship to the cluster states are still unclear and must be clarified to promote theoretical and experimental studies.

*masaaki@nucl.sci.hokudai.ac.jp

For this purpose, by using $\alpha + {}^{16}\text{O}$ and $\alpha + {}^{40}\text{Ca}$ cluster states in ${}^{20}\text{Ne}$ and ${}^{44}\text{Ti}$ as examples, we investigate the excitation mechanism of the IS dipole transition from the ground state to the asymmetric cluster states. We first discuss an analytic expression of the IS transition matrix from the shell-model ground state to the cluster states. It is found that the transition matrix is enlarged for asymmetric cluster systems and becomes as large as the Weisskopf estimate, even if the ground state is an ideal shell-model state. Furthermore, a simple numerical estimate using the Brink–Bloch wave function [57] shows that the matrix is considerably amplified if the ground state has cluster correlation.

To provide more realistic prediction of the IS dipole transition strength in ${}^{20}\text{Ne}$ and ${}^{44}\text{Ti}$, we also performed microscopic nuclear model calculations by using the generator coordinate method with the Brink–Bloch wave function (Brink–Bloch GCM) and antisymmetrized molecular dynamics (AMD) [58,59]. AMD is able to describe the distortion of the clusters and reasonably explains the observed excitation spectra of the ground band and cluster bands for both nuclei. The AMD result shows that only the 1^- states having the $\alpha + {}^{16}\text{O}$ or $\alpha + {}^{40}\text{Ca}$ cluster structure have a large transition matrix comparable to or larger than the Weisskopf estimate, and other non-cluster 1^- states are insensitive. From these results, we conclude that the IS dipole transition can strongly excite the 1^- cluster states and is a promising probe for asymmetric clustering when combined with the IS monopole transition that excites 0^+ cluster states.

This paper is organized as follows: In Sec. II, we derive an analytic expression for the IS dipole transition matrix. We also perform simple numerical estimation of the transition matrix using the Brink–Bloch wave function. The microscopic models, Brink–Bloch GCM and AMD, are introduced in Sec. III, and the results obtained with these models are discussed in Sec. IV. The final section summarizes this study.

II. ESTIMATES OF ISOSCALAR DIPOLE TRANSITION MATRIX

In this section, by using the shell-model and cluster-model wave functions, we estimate the magnitude of the IS dipole transition matrix between the ground and excited 1^- states of ${}^{20}\text{Ne}$ and ${}^{44}\text{Ti}$ having asymmetric cluster structure with $\alpha + {}^{16}\text{O}$ and $\alpha + {}^{40}\text{Ca}$ configurations.

By assuming that the ground state is described by a shell-model wave function, we first derive an analytical expression for the transition matrix and show that it is comparable with the Weisskopf estimate. We also show that the transition matrix is considerably amplified when the ground state has cluster correlation.

A. Analytical estimate of transition matrix

1. Wave functions of ground state and nodal and angular excited cluster states

The ground states of ${}^{20}\text{Ne}$ and ${}^{44}\text{Ti}$ are dominated by the $(0d1s)^4$ and $(0f1p)^4$ configurations on top of the closed-shell cores ${}^{16}\text{O}$ and ${}^{40}\text{Ca}$. The shell-model calculations [60–65]

showed that the ground state of ${}^{20}\text{Ne}$ is dominated by the SU(3) irreducible representation of $(\lambda, \mu) = (8, 0)$, and ${}^{44}\text{Ti}$ is by the $(12, 0)$ representation in the Elliott's SU(3) model [66]. An important fact here is that these shell-model wave functions are equivalently expressed by the $\alpha + {}^{16}\text{O}$ and $\alpha + {}^{40}\text{Ca}$ cluster-model wave functions owing to the Bayman–Bohr theorem [32]:

$$\Phi(\text{g.s.}) = \frac{c_0}{\sqrt{\mu_{N_0}}} \mathcal{A}' \{ \mathcal{R}_{N_0 0 0}(\mathbf{r}) \phi_1 \phi_2 \}, \quad (1)$$

$$c_0 = \sqrt{C_1! C_2! / A!},$$

$$\mu_N = \langle \mathcal{R}_{Nlm}(\mathbf{r}) \phi_1 \phi_2 | \mathcal{A}' \{ \mathcal{R}_{Nlm}(\mathbf{r}) \phi_1 \phi_2 \} \rangle. \quad (2)$$

Here, the internal wave functions of α cluster (with mass C_1) and ${}^{16}\text{O}$ or ${}^{40}\text{Ca}$ cluster (with mass C_2) denoted by ϕ_1, ϕ_2 are the harmonic oscillator wave functions with the oscillator parameter $\nu = m\omega/(2\hbar)$. The wave function of the intercluster motion is also the harmonic oscillator wave function $\mathcal{R}_{Nlm}(\mathbf{r}) = R_{Nl}(r) Y_{lm}(\hat{r})$ but its oscillator parameter is scaled by the reduced mass $\nu' = (C_1 C_2 / A) \nu$. The principal quantum number of the intercluster motion is equal to the lowest Pauli-allowed values: $N_0 = 8$ for ${}^{20}\text{Ne}$ and $N_0 = 12$ for ${}^{44}\text{Ti}$ [the nodal quantum numbers $n_0 = (N_0 - l)/2$ are 4 and 6].

As emphasized in Ref. [31], this equivalence of the shell-model and cluster-model wave functions implies that the degrees-of-freedom of cluster excitation are embedded even in an ideal shell-model ground state. For example, the nodal excitation of the intercluster motion yields the excited 0^+ state,

$$\Phi(0_{\text{ex}}^+) = \sum_{N=N_0+2}^{\infty} e_N \frac{c_0}{\sqrt{\mu_N}} \mathcal{A}' \{ \mathcal{R}_{N00}(\mathbf{r}) \phi_1 \phi_2 \}, \quad (3)$$

where the nodal quantum number of intercluster motion is increased relative to the ground state and, hence, the principal quantum number N must be equal to or larger than $N_0 + 2$. Thus, the states with larger values of N are coherently superposed with coefficients e_N . The 0_4^+ state of ${}^{20}\text{Ne}$ around 8.7 MeV [67] and 0^+ states of ${}^{44}\text{Ti}$ observed around 11 MeV [68,69] are attributed to this class of nodal excited cluster states. In Ref. [31], taking ${}^{12}\text{C}$ and ${}^{16}\text{O}$ as examples, it was shown that the IS monopole transition matrix from the ground state to the nodal excited cluster states is large.

Besides the nodal excitation, the angular excitation of the intercluster motion also takes place. For example, the angular excitation with $\Delta l = 1$ (combined with the nodal excitation) yields the 1^- state,

$$\Phi(1^-) = \sum_{N=N_0+1}^{\infty} f_N \frac{c_0}{\sqrt{\mu_N}} \mathcal{A}' \{ \mathcal{R}_{N10}(r) \phi_1 \phi_2 \}, \quad (4)$$

where the principal quantum number N must be equal to or larger than $N_0 + 1$. The 1_1^- state of ${}^{20}\text{Ne}$ at 5.8 MeV [67] and 1^- states of ${}^{44}\text{Ti}$ observed at 6.2 MeV and around 12 MeV [68–70] are attributed to this class of angular excited cluster state. Since the angular excitation with odd-number angular momenta (negative-parity states) is allowed only in the asymmetric cluster systems ($C_1 \neq C_2$), the 1^- state has been regarded as evidence of the asymmetric clustering [41].

2. Analytical expression of transition matrix

By using the wave functions described by Eqs. (1) and (4), we derive an analytic expression for the IS dipole transition between the ground and the angular excited 1^- cluster states. The IS dipole operator \mathcal{M}_μ^{IS1} , reduced matrix element M^{IS1} , and transition probability $B(IS1)$ are

$$\mathcal{M}_\mu^{IS1} = \sum_{i=1}^A (\mathbf{r}_i - \mathbf{r}_{c.m.})^2 \mathcal{Y}_{1\mu}(\mathbf{r}_i - \mathbf{r}_{c.m.}), \quad (5)$$

$$M^{IS1} = \langle 1^- || \mathcal{M}^{IS1} || 0_1^+ \rangle = \sqrt{3} \langle 1^-, J_z | \mathcal{M}_{J_z}^{IS1} | 0_1^+ \rangle, \quad (6)$$

$$B(IS1; 0_1^+ \rightarrow 1^-) = |M^{IS1}|^2, \quad (7)$$

where \mathbf{r}_i denotes the i th nucleon coordinate, while $\mathbf{r}_{c.m.}$ denotes the center of mass of the system. The solid spherical harmonics are defined as $\mathcal{Y}_{\lambda\mu}(\mathbf{r}) \equiv r^\lambda Y_{\lambda\mu}(\hat{r})$.

Applying the wave functions (1) and (4) to Eq. (6), the reduced matrix element is given as

$$\begin{aligned} M^{IS1} &= \sqrt{3} \langle \Phi(1^-) | \mathcal{M}_0^{IS1} | \Phi(g.s.) \rangle \\ &= \sum_{N=N_0+1} \frac{\sqrt{3} f_N}{\sqrt{\mu_{N_0} \mu_N}} \\ &\quad \times \langle \mathcal{M}_0^{IS1} \mathcal{R}_{N10}(\mathbf{r}) \phi_1 \phi_2 | \mathcal{A}' \{ \mathcal{R}_{N_00}(\mathbf{r}) \phi_1 \phi_2 \} \rangle. \end{aligned} \quad (8)$$

To evaluate the last matrix element, we rewrite \mathcal{M}_μ^{IS1} in terms of the internal coordinates ξ_i of each cluster and the intercluster coordinate \mathbf{r} , which are defined as

$$\mathbf{R}_{C_1} \equiv \frac{1}{C_1} \sum_{i \in C_1} \mathbf{r}_i, \quad \mathbf{R}_{C_2} \equiv \frac{1}{C_2} \sum_{i \in C_2} \mathbf{r}_i, \quad (9)$$

$$\xi_i \equiv \begin{cases} \mathbf{r}_i - \mathbf{R}_{C_1}, & i \in C_1 \\ \mathbf{r}_i - \mathbf{R}_{C_2}, & i \in C_2, \end{cases} \quad (10)$$

$$\mathbf{r} \equiv \mathbf{R}_{C_1} - \mathbf{R}_{C_2}, \quad (11)$$

where the center of mass of clusters \mathbf{R}_{C_1} and \mathbf{R}_{C_2} are introduced. With these coordinates, as explained in Appendix A, \mathcal{M}_μ^{IS1} is expressed as

$$\begin{aligned} \mathcal{M}_\mu^{IS1} &= \sum_{i \in C_1} \xi_i^2 \mathcal{Y}_{1\mu}(\xi_i) + \sum_{i \in C_2} \xi_i^2 \mathcal{Y}_{1\mu}(\xi_i) - \sqrt{\frac{32\pi}{9}} \left\{ \frac{C_2}{A} \left[\sum_{i \in C_1} \mathcal{Y}_2(\xi_i) \otimes \mathcal{Y}_1(\mathbf{r}) \right]_{1\mu} - \frac{C_1}{A} \left[\sum_{i \in C_2} \mathcal{Y}_2(\xi_i) \otimes \mathcal{Y}_1(\mathbf{r}) \right]_{1\mu} \right\} \\ &\quad + \frac{5}{3} \left(\frac{C_2}{A} \sum_{i \in C_1} \xi_i^2 - \frac{C_1}{A} \sum_{i \in C_2} \xi_i^2 \right) \mathcal{Y}_{1\mu}(\mathbf{r}) - \frac{C_1 C_2 (C_1 - C_2)}{A^2} r^2 \mathcal{Y}_{1\mu}(\mathbf{r}). \end{aligned} \quad (12)$$

This expression makes it clear that \mathcal{M}_μ^{IS1} will activate the degrees of freedom of cluster excitation embedded in the ground state. It will generate angular excited cluster states with $J^\pi = 1^-$, because if operated on the ground-state wave function given in Eq. (1), the terms depending on $\mathcal{Y}_{1\mu}(\mathbf{r})$ and $r^2 \mathcal{Y}_{1\mu}(\mathbf{r})$ will induce the nodal and angular excitation of the intercluster motion.

By substituting Eq. (12) into Eq. (8), one finds that the first line of Eq. (12) identically vanishes because it involves the internal excitation of clusters. Hence, only the second line has nonvanishing matrix element, as given below (see Appendix B for the derivation):

$$\begin{aligned} M^{IS1} &= \sqrt{\frac{3}{4\pi}} \frac{C_1 C_2}{A} \left[f_{N_0+1} \sqrt{\frac{\mu_{N_0}}{\mu_{N_0+1}}} \left\{ \frac{5}{3} (\langle r^2 \rangle_{C_1} - \langle r^2 \rangle_{C_2}) \langle R_{N_00} | r | R_{N_0+11} \rangle - \frac{C_1 - C_2}{A} \langle R_{N_00} | r^3 | R_{N_0+11} \rangle \right\} \right. \\ &\quad \left. - \frac{C_1 - C_2}{A} f_{N_0+3} \sqrt{\frac{\mu_{N_0}}{\mu_{N_0+3}}} \langle R_{N_00} | r^3 | R_{N_0+31} \rangle \right], \end{aligned} \quad (13)$$

where $\langle r^2 \rangle_{C_1}$ and $\langle r^2 \rangle_{C_2}$ are the square of the root-mean-square radius of the clusters, and the matrix elements of the harmonic oscillator are given as

$$\begin{aligned} \langle R_{N_00} | r | R_{N_0+11} \rangle &= \sqrt{\frac{N_0 + 3}{4\nu'}}, \\ \langle R_{N_00} | r^3 | R_{N_0+11} \rangle &= \frac{3N_0 + 5}{4\nu'} \sqrt{\frac{N_0 + 3}{4\nu'}}, \\ \langle R_{N_00} | r^3 | R_{N_0+31} \rangle &= -\frac{\sqrt{(N_0 + 2)(N_0 + 5)}}{4\nu'} \sqrt{\frac{N_0 + 3}{4\nu'}}. \end{aligned} \quad (14)$$

From Eqs. (13) and (14), we find following properties: (1) The transition matrix is proportional to $\langle r^2 \rangle_{C_1} - \langle r^2 \rangle_{C_2}$ or $(C_1 - C_2)/A$, which means that it is amplified for the

asymmetric cluster states. Therefore, we expect that the IS dipole transition is a good probe for asymmetric clustering. (2) For the cluster states dominated by the $1\hbar\omega$ configuration, the first line of Eq. (13) dominantly contributes, while the second line becomes major for the $3\hbar\omega$ excited cluster states. (3) From Eq. (14), the matrix element becomes larger as the oscillator parameter ν' decreases, which means an increase in the size of the relative wave function and in the intercluster distance.

3. Estimate of matrix element

We are now able to estimate the magnitude of the IS dipole transition matrix. We adopted the values listed in Table I. Here, the oscillator parameters $\nu = 0.16 \text{ fm}^{-2}$ for ^{20}Ne and 0.12 fm^{-2} for ^{44}Ti are determined to minimize

TABLE I. List of the quantities used to evaluate Eq. (13). Radii of α , ^{16}O , and ^{40}Ca clusters are calculated from the measured charge radii given in Ref. [71] and listed in units of fm^2 . The oscillator parameters ν and ν' are in units of fm^{-2} . Other quantities are dimensionless.

	N_0	$\mu_{N_0}^a$	μ_{N_0+1}	μ_{N_0+3}	$\langle r^2 \rangle_{C_1}$	$\langle r^2 \rangle_{C_2}$
^{20}Ne	8	0.229	0.344	0.620	$(1.46)^2$	$(2.57)^2$
^{44}Ti	12	0.069	0.157	0.372	$(1.46)^2$	$(3.37)^2$
	ν	ν'	f_{N_0+1}	f_{N_0+3}		
^{20}Ne	0.16	0.51	$\sqrt{0.39}$	$-\sqrt{0.28}$		
^{44}Ti	0.12	0.44	$\sqrt{0.23}$	$-\sqrt{0.26}$		

^a μ_N defined in Eq. (2) is the so-called eigenvalue of the RGM norm kernel and is analytically calculable. The values listed in the table are taken from Ref. [72].

the ground-state energies as explained in Sec. III. And the oscillator parameter of the relative wave function is scaled by the reduced mass as $\nu' = C_1 C_2 \nu / A$. The coefficients f_{N_0+1} and f_{N_0+3} are estimated by the AMD calculation, which is also explained in Sec. III. For other quantities, an analytical calculation is possible or an experimental value is available. Assignment of those values to Eq. (13) yields the estimate of ^{20}Ne :

$$M^{\text{IS}1}(^{20}\text{Ne}) = 3.08 f_9 - 7.36 f_{11} = 5.82 \text{ fm}^3, \quad (15)$$

and for ^{44}Ti ,

$$M^{\text{IS}1}(^{44}\text{Ti}) = 13.3 f_{13} - 16.2 f_{15} = 14.6 \text{ fm}^3. \quad (16)$$

Note that f_{N_0+1} and f_{N_0+3} usually have opposite signs for angular excited cluster states, as explained in Appendix C, so the first and second terms in Eqs. (15) and (16) contribute additively to enlarge the matrix element.

These results are compared with the single-particle estimates. Assuming a constant radial wave function as usual, the Weisskopf estimate is given as

$$M_{\text{WU}}^{\text{IS}1} = \sqrt{\frac{3}{4\pi}} \frac{3}{6} (1.2A^{1/3})^3 \simeq 0.422A \text{ fm}^3. \quad (17)$$

It is approximately 8.44 fm^3 for ^{20}Ne and 18.6 fm^3 for ^{44}Ti , which are slightly larger than but comparable to Eqs. (15) and (16).

Thus, the angular excited cluster states have a strong IS dipole transition from the ground state comparable to the Weisskopf estimate, even if the ground state is not a cluster state but an ideal shell-model state. Since the single-particle transition is usually fragmented into many states, only the asymmetric cluster states can have strong transition strengths. Furthermore, as we will show below, the strength is further amplified if the ground state has cluster correlation.

B. Amplification of transition matrix owing to clustering of ground state

Here we show that the magnitude of $M^{\text{IS}1}$ is considerably amplified compared with the estimates made in the previous section if the ground state has cluster correlation. To demonstrate this, we employ Brink–Bloch wave function [57], which

is composed of clusters C_1 and C_2 placed at $-C_2/AD$ and C_1/AD with the intercluster distance D ,

$$\Phi_{\text{BB}}(D) = n_0 \mathcal{A}' \left\{ \psi_{C_1} \left(-\frac{C_2}{A} \mathbf{D} \right) \psi_{C_2} \left(\frac{C_1}{A} \mathbf{D} \right) \right\}, \quad (18)$$

$$\mathbf{D} = (0, 0, D),$$

where ψ_{C_1} and ψ_{C_2} denote the wave functions of clusters represented by the harmonic oscillator wave functions that include their center-of-mass coordinates. The oscillator parameters are $\nu = 0.16$ and 0.12 fm^{-2} for ^{20}Ne and ^{44}Ti , respectively. Equation (18) is projected onto the eigenstate of parity and angular momentum,

$$\Phi_{\text{BB}}^\pi(D) = \frac{1 + \pi P_x}{2} \Phi_{\text{BB}}(D), \quad \pi = \pm, \quad (19)$$

$$\Phi_{\text{BB}}^{l\pi}(D) = \frac{2l+1}{8\pi^2} \int d\Omega D_{M0}^{l*}(\Omega) R(\Omega) \Phi_{\text{BB}}^\pi(D). \quad (20)$$

Here P_x , $D_{MK}^l(\Omega)$, and $R(\Omega)$ denote the parity operator, the Wigner D function, and the rotation operator. It is known that the Brink–Bloch wave function can be transformed into the form of Eqs. (1), (3), and (4) [72],

$$\Phi_{\text{BB}}^{l\pi}(D) = \phi_{\text{c.m.}}(\mathbf{r}_{\text{c.m.}}) n_0 \mathcal{A}' \{ \chi_{\text{BB}}(\mathbf{r}) \phi_1 \phi_2 \}, \quad (21)$$

$$\phi_{\text{c.m.}}(\mathbf{r}_{\text{c.m.}}) = \left(\frac{2Av}{\pi} \right)^{3/4} e^{-Avr_{\text{c.m.}}^2},$$

$$\chi_{\text{BB}}(\mathbf{r}) = \sum_N A_{Nl} \frac{(v'D^2)^{N/2}}{\sqrt{N!}} e^{-v'D^2/2} \mathcal{R}_{Nl0}(\mathbf{r}), \quad (22)$$

$$A_{Nl} = (-)^{(N-l)/2} \sqrt{\frac{(2l+1)N!}{(N-l)!(N+l+1)!}}, \quad (23)$$

where $\phi_{\text{c.m.}}(\mathbf{r}_{\text{c.m.}})$ is the center-of-mass wave function, and the wave function of the intercluster motion $\chi_{\text{BB}}(\mathbf{r})$ is expanded by the harmonic oscillator wave functions. From this expression, we can see that Brink–Bloch wave function becomes identical to Eq. (1) in the limit $D \rightarrow 0$ and, hence, equals the shell-model wave function. Of course, as D increases, the wave function exhibits stronger clustering.

By using the Brink–Bloch wave functions for $\alpha + ^{16}\text{O}$ (^{20}Ne) and $\alpha + ^{40}\text{Ca}$ (^{44}Ti) systems, we calculated the transition matrix:

$$M_{\text{BB}}^{\text{IS}1}(D_0, D_1) = \frac{\sqrt{3} \langle \Phi_{\text{BB}}^{1-}(D_1) | \mathcal{M}_0^{\text{IS}1} | \Phi_{\text{BB}}^{0+}(D_0) \rangle}{\sqrt{\langle \Phi_{\text{BB}}^{0+}(D_0) | \Phi_{\text{BB}}^{0+}(D_0) \rangle \langle \Phi_{\text{BB}}^{1-}(D_1) | \Phi_{\text{BB}}^{1-}(D_1) \rangle}}. \quad (24)$$

The result is shown in Fig. 1 where the ratio of the transition matrix to the Weisskopf estimate given by Eq. (17) is plotted as function of the intercluster distances D_0 in the ground state and D_1 in the 1^- state. In both systems, we see that, even for small values of D_0 and D_1 , $M_{\text{BB}}^{\text{IS}1}$ is larger than the Weisskopf estimates. It is impressive that the matrix element is considerably amplified as both D_0 and D_1 increase.

By the more detailed calculations explained in the next section, the position of the ground and 1^- states are estimated

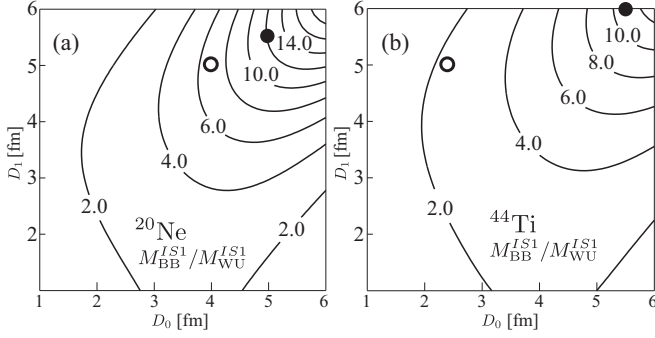


FIG. 1. The ratio of the transition matrix to the Weisskopf estimate, $M_{\text{BB}}^{\text{IS1}}/M_{\text{WU}}^{\text{IS1}}$, as function of the intercluster distances in the ground state D_0 and in the 1^- state D_1 . Panel (a) is for the $\alpha + {}^{16}\text{O}$ (${}^{20}\text{Ne}$) system, while panel (b) is for the $\alpha + {}^{40}\text{Ca}$ (${}^{44}\text{Ti}$) system. The circles show the approximate positions of the ground and excited 1^- states obtained by the Brink–Bloch GCM (filled circles) and AMD (open circles) calculations given in Sec. IV.

approximately at the open circles in Fig. 1. Therefore, the transition strength is indeed considerably amplified and regarded as a good probe for asymmetric clustering.

III. MICROSCOPIC NUCLEAR MODELS

To provide realistic and reliable results for the IS dipole transition of ${}^{20}\text{Ne}$ and ${}^{44}\text{Ti}$, we performed two microscopic nuclear model calculations which we explain in this section. The first is the Brink–Bloch GCM and the other is AMD. The Brink–Bloch GCM can properly describe the intercluster motion. In addition to this, AMD can also describe the polarization and distortion of clusters.

In both theoretical models, the following microscopic A -body Hamiltonian is commonly used:

$$H = \sum_{i=1}^A t(i) + \sum_{i<j}^A v_n(ij) + \sum_{i<j}^Z v_C(ij) - t_{\text{c.m.}}, \quad (25)$$

where the Gogny $D1S$ interaction [73] is used as an effective nucleon-nucleon interaction v_n . The Coulomb interaction v_C is approximated by a sum of seven Gaussians. The center-of-mass kinetic energy $t_{\text{c.m.}}$ is exactly removed.

A. Generator coordinate method with Brink–Bloch wave function

The Brink–Bloch GCM uses Eq. (20) as the basis function and employs the intercluster distance D as generator coordinate. The width parameter ν is so chosen to minimize the ground-state energy, which is found to be $\nu = 0.16$ and 0.12 fm^{-2} for ${}^{20}\text{Ne}$ and ${}^{44}\text{Ti}$, respectively. In the practical calculation, D is discretized ranging from 1.0 to 12.0 fm with an interval of 0.5 fm, which generates 23 basis functions $\Phi_{\text{BB}}^{l\pi}(D_i)$, $i = 1, \dots, 23$.

To describe the ground and $\alpha + {}^{16}\text{O}$ cluster states, the basis functions are superposed,

$$\Psi_{M_p}^{l\pi} = \sum_i g_{i p} \Phi_{\text{BB}}^{l\pi}(D_i). \quad (26)$$

By solving the following Griffin–Hill–Wheeler equation [74,75], we obtain the eigenenergy E_p and the coefficients of the superposition $g_{i p}$:

$$\sum_{i'} H_{ii'}^{l\pi} g_{i' p} = E_p^{l\pi} \sum_{i'} N_{ii'}^{l\pi} g_{i' p}, \quad (27)$$

$$H_{ii'}^{l\pi} = \langle \Phi_{\text{BB}}^{l\pi}(D_i) | \hat{H} | \Phi_{\text{BB}}^{l\pi}(D_{i'}) \rangle, \quad (28)$$

$$N_{ii'}^{l\pi} = \langle \Phi_{\text{BB}}^{l\pi}(D_i) | \Phi_{\text{BB}}^{l\pi}(D_{i'}) \rangle. \quad (29)$$

By using the thus-obtained wave functions for the ground and excited 1^- states, the reduced matrix element given in Eq. (6) is directly calculated.

B. Antisymmetrized molecular dynamics

In the AMD model [58,59], each nucleon is represented by a localized Gaussian wave packet,

$$\varphi_i(\mathbf{r}) = \exp \left\{ - \sum_{\sigma=x,y,z} v_{\sigma} \left(r_{\sigma} - \frac{Z_{i\sigma}}{\sqrt{v_{\sigma}}} \right)^2 \right\} \chi_i \xi_i, \quad (30)$$

$$\chi_i = a_i \chi_{\uparrow} + b_i \chi_{\downarrow}, \quad \xi_i = \text{proton or neutron},$$

where χ_i and ξ_i represent spin and isospin wave functions, respectively. The intrinsic wave function is a Slater determinant of nucleon wave packets,

$$\Phi_{\text{int}} = \mathcal{A}\{\varphi_1 \varphi_2 \cdots \varphi_A\}. \quad (31)$$

The parameters of the intrinsic wave function, \mathbf{Z}_i , a_i , b_i , and v_{σ} , are determined by the energy minimization explained below.

Before the energy minimization, the intrinsic wave function is projected to the eigenstate of the parity,

$$\Phi^{\pi} = \frac{1 + \pi P_x}{2} \Phi_{\text{int}}, \quad \pi = \pm. \quad (32)$$

Then, the above-mentioned parameters are determined to minimize the expectation value of the Hamiltonian \tilde{E} that is defined as

$$\tilde{E} = \frac{\langle \Phi^{\pi} | \hat{H} | \Phi^{\pi} \rangle}{\langle \Phi^{\pi} | \Phi^{\pi} \rangle} + V_c, \quad (33)$$

$$V_c = v_{\beta}(\langle \beta \rangle - \beta_0)^2 + v_{\gamma}(\langle \gamma \rangle - \gamma_0)^2. \quad (34)$$

Here the potential V_c is added to impose the constraint on the quadrupole deformation of intrinsic wave function that is parametrized by $\langle \beta \rangle$ and $\langle \gamma \rangle$ as defined in Ref. [76]. The magnitudes of v_{β} and v_{γ} are chosen large enough so that $\langle \beta \rangle$ and $\langle \gamma \rangle$ are, after the energy minimization, equal to β_0 and γ_0 , respectively. By the energy minimization, we obtain the optimized wave function $\Phi_{\text{int}}^{\pi}(\beta_0, \gamma_0)$ for discretized sets of (β_0, γ_0) on the triangular lattice in β - γ plane. The lattice size is 0.05 and the calculation is performed up to $\beta = 0.9$.

After the energy minimization, we project out an eigenstate of angular momentum and perform the GCM calculation by using the quadrupole deformation parameters β_0 and γ_0 as the generator coordinates. We also included the Brink–Bloch wave functions $\Phi_{\text{BB}}^{l\pi}(D_i)$ as the basis functions of GCM. For simplicity, we denote by Φ_i this set of basis functions. Because the AMD wave function is not necessarily axially symmetric,

nonzero values of K quantum number and their mixing must be taken into account. Hence the equation for the angular momentum projection and the Griffin–Hill–Wheeler equation are

$$\Phi_{MKi}^{J\pi} = \frac{2J+1}{8\pi^2} \int d\Omega D_{MK}^{J*}(\Omega) \hat{R}(\Omega) \Phi_i^\pi, \quad (35)$$

and

$$\Psi_{Mp}^{J\pi} = \sum_{Ki} g_{Kip} \Phi_{MKi}^{J\pi}, \quad (36)$$

$$\sum_{i'K'} H_{KiK'i'}^{J\pi} g_{K'i'p} = E_p^{J\pi} \sum_{i'K'} N_{KiK'i'}^{J\pi} g_{K'i'p}, \quad (37)$$

$$H_{KiK'i'}^{J\pi} = \langle \Phi_{MKi}^{J\pi} | \hat{H} | \Phi_{MK'i'}^{J\pi} \rangle, \quad (38)$$

$$N_{KiK'i'}^{J\pi} = \langle \Phi_{MKi}^{J\pi} | \Phi_{MK'i'}^{J\pi} \rangle. \quad (39)$$

By using the wave function given in Eq. (36) the transition matrix element is calculated.

For a better understanding of the results presented in the next section, it is helpful to note the differences between the Brink–Bloch GCM and AMD. First, because nucleons are treated as independent wave packets, AMD is able to describe various the non-cluster states as well as the cluster states, while the Brink–Bloch GCM is not. Second, for the same reason, AMD is capable of describing the polarization and distortion of clusters. Finally, since the Brink–Bloch wave functions are also employed as the basis function, the AMD includes the Brink–Bloch GCM as a part of its model space. In short, in the AMD, the distortion of clusters and the coupling between the cluster states and non-cluster states are taken into account.

C. Projection of antisymmetrized-molecular-dynamics wave function to Brink–Bloch wave function

As explained above, the AMD wave function is an admixture of the cluster and non-cluster wave functions. To identify the cluster state from AMD results, it is convenient to introduce an approximate projector to the Brink–Bloch wave function,

$$P_{BB} = \sum_{ij} |\Phi_{BB}^{J\pi}(D_i)\rangle \langle B^{-1} \rangle_{ij} \langle \Phi_{BB}^{J\pi}(D_j) |, \quad (40)$$

where B^{-1} is the inverse of the overlap matrix B defined as $B_{ij} = \langle \Phi_{BB}^{J\pi}(D_i) | \Phi_{BB}^{J\pi}(D_j) \rangle$. With this projector, the AMD wave function (36) is projected onto Brink–Bloch wave function,

$$P_{BB} \Psi_{Mp}^{J\pi} = \sum_i G_i \Phi_{BB}^{J\pi}(D_i), \quad (41)$$

$$G_i = \sum_j \langle B^{-1} \rangle_{ij} \langle \Phi_{BB}^{J\pi}(D_j) | \Psi_{Mp}^{J\pi} \rangle. \quad (42)$$

By substituting Eqs. (21)–(23) into the right-hand side of Eq. (41) and by comparing it with Eq. (4), we calculated the coefficient of superposition f_{N_0+1} and f_{N_0+3} given in Table I. The projector is also used to evaluate the amount of the cluster component in the AMD wave function, which is defined as

$$S = \langle \Psi_{Mp}^{J\pi} | P_{BB} | \Psi_{Mp}^{J\pi} \rangle. \quad (43)$$

When this value is sufficiently large, the excited state may be regarded as a cluster state.

We also explain how we estimated the intercluster distances D_0 and D_1 which are shown by circles in Fig. 1. We calculate the overlap between the GCM wave functions $\Psi_{Mp}^{J\pi}$ for the ground and 1^- states and the Brink–Bloch wave function $\Phi_{BB}^{J\pi}(D_i)$,

$$\frac{|\langle \Psi_{Mp}^{J\pi} | \Phi_{BB}^{J\pi}(D_i) \rangle|^2}{\langle \Phi_{BB}^{J\pi}(D_i) | \Phi_{BB}^{J\pi}(D_i) \rangle},$$

and regard the distance D_i at which the overlap has its maximum as D_0 or D_1 .

IV. MICROSCOPIC MODEL CALCULATIONS FOR ISOSCALAR DIPOLE TRANSITION

In this section, we discuss the IS dipole transitions in ^{20}Ne and ^{44}Ti studied by Brink–Bloch GCM and AMD. In Refs. [77–79], the cluster and non-cluster states of ^{20}Ne and ^{44}Ti have already been discussed based on the AMD calculation, and the reader is directed to those references for more detail. Here we focus on the $\alpha + ^{16}\text{O}$ and $\alpha + ^{40}\text{Ca}$ cluster states and discuss the IS dipole transitions from the ground state to those cluster states.

A. $\alpha + ^{16}\text{O}$ cluster states in ^{20}Ne

The $\alpha + ^{16}\text{O}$ cluster states in ^{20}Ne have been studied in detail by many authors [77,78,80–88] and well established.

The observed $\alpha + ^{16}\text{O}$ cluster bands are summarized in Fig. 2 together with the results of Brink–Bloch GCM and AMD. The 0_4^+ state observed at 8.7 MeV (4 MeV above the α threshold) has large α decay width comparable with the Wigner limit and is known as the nodal excited cluster state described by the wave function of Eq. (3). A rotational band is built on this state, which hereafter we call the “nodal excited band.” The 1_1^- state at 5.8 MeV (1.1 MeV above the α threshold) also has large α decay width and is known as the angular excited cluster state described by the wave function of Eq. (4). This 1_1^- state is of particular importance because it is regarded as the evidence for the asymmetric clustering with the $\alpha + ^{16}\text{O}$ configuration. On this state, the negative-parity band is built.

It is well known that the ground band is the positive-parity partner of the negative-parity band, and those two bands constitute the parity doublet [41]. This means that the ground state has non-negligible cluster correlation. Therefore, on the basis of the discussion made in in Sec. II B, we expect that the IS dipole transition to the 1_1^- state is considerably amplified.

Next, we examine the theoretical results. In the case of ^{20}Ne , it was easy to identify the $\alpha + ^{16}\text{O}$ cluster states from the AMD results, because all of the states shown in Fig. 2 have large values of S defined in Eq. (43). For example, $S = 0.69, 0.90,$ and 0.81 for the ground, 1_1^- , and 0_4^+ states, respectively.

It is interesting to note the difference between the Brink–Bloch GCM and AMD results. The Brink–Bloch GCM fails to reproduce the energy of the ground band, while AMD reasonably describes it, that indicates the importance of the

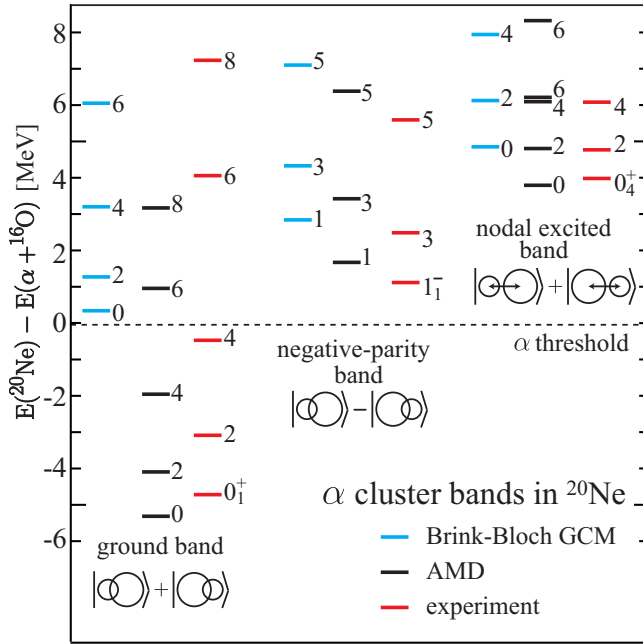


FIG. 2. The observed and calculated $\alpha + {}^{16}\text{O}$ cluster states in ${}^{20}\text{Ne}$ classified into three rotational bands. Energy is measured from the α threshold located at 4.7 MeV above the ground state. In the AMD result, the 6^+ member state of the nodal excited band is fragmented into two states due to the coupling with non-cluster configurations.

cluster distortion effect. As discussed in the AMD study [77], the spin-orbit interaction and the formation of mean field dissolve the α cluster. As a result, the radius of the ground state is reduced to 2.98 fm in AMD from 3.27 fm in Brink–Bloch GCM. They also reduces the estimated intercluster distance D in AMD as listed in Table II. Hence, the overlap between the ground-state wave functions of AMD and Brink–Bloch GCM is not large and is approximately 46%. On the other hand, both theoretical models give reasonable description for negative-parity and nodal excited bands. Therefore, we can regard that the distortion effect is less important and almost ideal clustering is realized in the 0_4^+ and 1_1^- states, for which both theoretical models yielded large intercluster distances. For example, the radius of the 1_1^- state calculated by AMD and Brink–Bloch GCM are close to each other (3.26 fm in AMD and 3.33 fm in Brink–Bloch GCM) and their wave functions have large overlap amounting to 87%.

The calculated IS dipole transition matrix from the ground state to the 1_1^- states are listed in Table II. It is evident that

TABLE II. The estimated intercluster distance of the ground and the $\alpha + {}^{16}\text{O}$ cluster states in units of fm, and the IS dipole and monopole transition matrix from the ground state to the 1_1^- and 0_4^+ states in units of fm^3 and fm^2 . Numbers in parentheses are the ratio to the Weisskopf estimates.

	D_0	D_1	$D(0_4^+)$	$M^{\text{IS}1}$	$M^{\text{IS}0}$
Brink–Bloch GCM	5.0	5.5	6.5	90.2 (10.7)	46.4 (7.3)
AMD	4.0	5.0	6.0	38.0 (4.5)	16.0 (2.5)

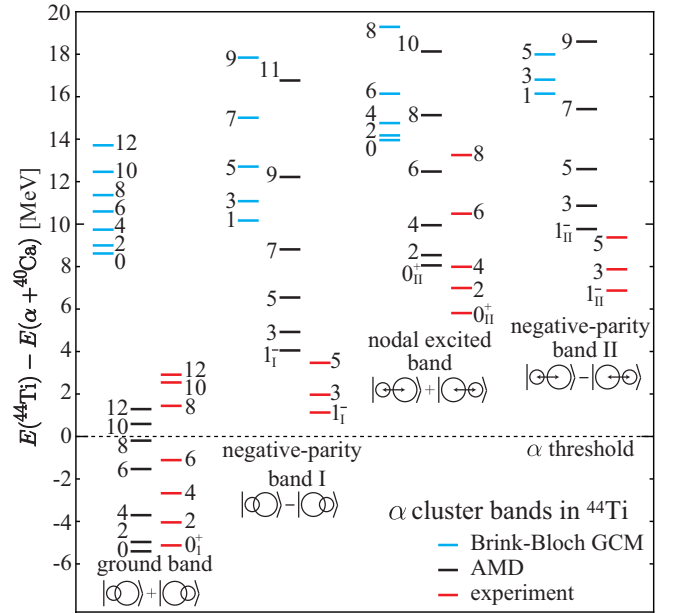


FIG. 3. The observed and calculated $\alpha + {}^{40}\text{Ca}$ cluster states in ${}^{44}\text{Ti}$ classified into four rotational bands. Energy is measured from the α threshold located at 5.1 MeV above the ground state. In the experiment and AMD results, the member states of the nodal excited band and negative-parity band II are fragmented into several levels, and the weighted averages of those levels are shown in the figure.

the transition is greatly enhanced compared to Weisskopf estimates. In particular, Brink–Bloch GCM yielded huge values, which is due to the too-weak binding of the ground state leading to the overestimate of the radius and cluster correlation of the ground state. If the cluster-distortion effect is taken into account by AMD, the strength is somewhat reduced but still much larger than the Weisskopf estimate. We also note that the nodal excited state (0_4^+) has a large monopole transition matrix, as expected. Therefore, the present results suggest that both of the positive- and negative-parity cluster states can be strongly generated by the IS monopole and dipole transitions from the ground state and, hence, those transitions will be good signatures of the asymmetric clustering.

B. $\alpha + {}^{40}\text{Ca}$ cluster states in ${}^{44}\text{Ti}$

The $\alpha + {}^{40}\text{Ca}$ cluster states in ${}^{44}\text{Ti}$ have also been studied by many authors [68–70,79,89–98], but the situation is more complicated than the case of ${}^{20}\text{Ne}$. The theoretical and experimental studies are summarized in a review paper [99], and our discussion is based on the assignment given therein.

Figure 3 shows the observed candidates of $\alpha + {}^{40}\text{Ca}$ cluster states together with the present theoretical results. Based on the α -transfer experiment, four rotational bands including the ground band were classified as $\alpha + {}^{40}\text{Ca}$ cluster bands. The 1_1^- state observed at 6.2 MeV (1.1 MeV above the α threshold) is strongly populated by the α -transfer reaction [70,89] and is the angular excited cluster state dominated by the $1\hbar\omega$ excitation of the intercluster motion. Although it is not the yrast 1_1^- state, we call this state the 1_1^- state in the following. On this 1_1^- state,

a rotational band which we call the “negative-parity band I” is built.

A couple of candidates of the nodal excited 0^+ state are reported around 11.0 MeV (5.9 MeV above the α threshold) by the α elastic scattering [94] and the α -transfer reaction [68,69,89]. Those data suggest that the nodal excited cluster state may be fragmented into several states due to the coupling with other non-cluster configurations. In Fig. 3, by taking the average, the nodal excited state is plotted as a single state which we call the 0_{II}^+ state. On this 0_{II}^+ state the nodal excited band is built.

Around 12 MeV in excitation energy, another group of 1^- states having large α spectroscopic factors are reported [68,69,89]. Again, observed α spectroscopic factors are fragmented into several levels and the averaged value which we call the 1_{II}^- state is shown in the figure. Although the assignment is not so firm, another negative-parity band is suggested on this state which we denote by “negative-parity band II.” The excitation energy of this band plausibly agrees with the cluster-model calculation which suggests the $3\hbar\omega$ excitation of the intercluster motion.

The information on the $\alpha + {}^{40}\text{Ca}$ cluster states is summarized as follows: First, the ground and the negative-parity band I built on the 1_1^- state at 6.2 MeV constitute a parity doublet. Second, the nodal excited band built on the 0_{II}^+ state around 11 MeV and the negative-parity band II on the 1_{II}^- state around 12 MeV may constitute another parity doublet. The first doublet is dominated by the 0 and $1\hbar\omega$ excitations of the intercluster motion, while the second doublet is dominated by the $2\hbar\omega$ and $3\hbar\omega$ excitations.

Next, we discuss the results of the Brink–Bloch GCM. The Brink–Bloch GCM seriously overestimates the energies of the observed cluster bands as well as the ground band. This is because of the neglect of the spin-orbit interaction and the formation of mean field which considerably dissolves α cluster in ${}^{44}\text{Ti}$ and gains additional binding energy [79]. Indeed, if we take into account those effects by using AMD, the ground-state radius is decreased to 3.52 fm from 3.68 fm in Brink–Bloch GCM, and the intercluster distance D is also considerably decreased, as listed in Table III. As a result, the overlap between the ground-state wave functions of AMD and Brink–Bloch GCM is as small as 29%. Because of too-large

TABLE III. The estimated intercluster distance of the ground and the $\alpha + {}^{40}\text{Ca}$ cluster states in units of fm, and the IS dipole and monopole transition matrix from the ground state to the 1_1^- , 1_{II}^- , and 0_{II}^+ states in units of fm^3 and fm^2 . Intercluster distances $D(0_{\text{II}}^+)$ and $D(1_{\text{II}}^-)$ are the averaged values of the fragmented levels, while the transition matrix $M^{\text{IS}0}(0_{\text{II}}^+)$ and $M^{\text{IS}1}(1_{\text{II}}^-)$ are their sum. Numbers in parentheses are the ratio to the Weisskopf estimates.

	D_0	D_{I}	$D(0_{\text{II}}^+)$	$D(1_{\text{II}}^-)$
Brink–Bloch GCM	5.5	6.0	7.0	7.5
AMD	2.5	5.0	6.0	7.0
	$M^{\text{IS}1}(1_1^-)$	$M^{\text{IS}0}(0_{\text{II}}^+)$	$M^{\text{IS}1}(1_{\text{II}}^-)$	
Brink–Bloch GCM	217.5 (11.7)	47.2 (4.4)	91.6 (4.9)	
AMD	24.7 (1.3)	19.9 (1.8)	16.7 (0.9)	

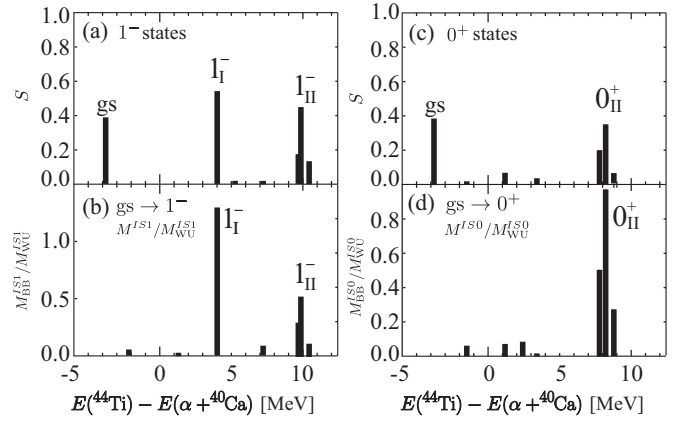


FIG. 4. (a) The amount of the cluster component S of the ground and 1^- states obtained by AMD. (b) The ratio of IS dipole transition matrix $M^{\text{IS}1}$ to the Weisskopf estimate. (c) Same as panel (a) but for the 0^+ states. (d) Same as panel (b) but for the IS monopole transition.

intercluster distance, Brink–Bloch GCM yields the huge dipole and monopole transition matrix listed in Table III which may be over-amplified and unrealistic.

In the AMD results, the member states of the nodal excited band and negative-parity band II are fragmented into several states, as reported by experiment. Therefore, for the states shown in Fig. 3 and the intercluster distances listed in Table III, we show the averaged values weighted by the amount of the cluster component S given by Eq. (43). By taking the distortion effect into account, AMD gives a reasonable description of the ground and cluster bands. All states gain large binding energy compared with the Brink–Bloch GCM, and their intercluster distances, in particular that of the ground state, are considerably reduced. This strong distortion is mainly due to the spin-orbit interaction and to the formation of the mean field.

Since the nodal excited band and the negative-parity band II are fragmented, we discuss the transition matrix by referring to the distribution of the amount of the cluster component S . Figure 4(a) shows S of the ground and 1^- states as function of energy relative to the α threshold. The ground state has, despite the strong cluster distortion, a considerable amount of cluster component $S = 0.39$. However, we note that this does not necessarily mean prominent clustering in the ground state. Most of this cluster component is the wave function given in Eq. (1) and hence is identical to the shell-model wave function. The first angular excited state (the 1_1^- state), located 4 MeV above the threshold, has a larger value of $S = 0.59$. The second angular excited state (the 1_{II}^- state) is fragmented into three levels around 10 MeV above the threshold. If we sum up those fragments, it amounts to $S = 0.78$. The IS dipole transition matrix from the ground state to 1^- states is shown in Fig. 4(b). It is clear that both of the angular excited states are strongly excited, because the IS dipole transition brings about $1\hbar\omega$ and $3\hbar\omega$ excitation of the intercluster motion, as shown by Eq. (12). It must be noted that many non-cluster 1^- states are obtained between the ground and 1_{II}^- states in the AMD calculation, but none of them have a transition matrix comparable to the Weisskopf estimate. This result shows that

the IS dipole transition is sensitive to angular excited 1^- states, despite the cluster distortion and fragmentation.

As for the 0^+ states and the monopole transition, almost the same conclusion can be drawn. Figure 4(c) shows the amount of cluster component in the 0^+ states. Around 8 MeV, the nodal excited 0_{II}^+ state is fragmented into three levels, which amount to $S = 0.6$. Again, we see the amount of cluster component S and transition matrix are strongly correlated. The nodal excited states have large IS monopole transition matrix, while non-cluster states are insensitive. From those results, we conclude that the IS monopole and dipole transitions are good probes for asymmetric clustering. Since both transitions can be measured simultaneously by α inelastic scattering, the experimental and theoretical survey looks promising.

We also comment on the giant resonances, which may exist at an energy region similar to that of the 1_{II}^- and 0_{II}^+ states. Because the peak of the giant resonance may overlap with those states, those nodal excited doublets may not be visible in the real situation. Nevertheless, we expect that it is possible to identify those cluster states, because they will dominantly decay by α emission, while the giant resonance decays by neutron emission.

V. SUMMARY

In this study, we have discussed the IS dipole transitions in ^{20}Ne and ^{44}Ti that have $\alpha + ^{16}\text{O}$ and $\alpha + ^{40}\text{Ca}$ cluster states. In such asymmetric-cluster systems, the existence of the angular excited 1^- cluster states is a key to prove their asymmetric structure. We have shown that the isoscalar dipole transition from the ground state strongly populates those asymmetric cluster states and, hence, it is regarded as a good probe for such 1^- states.

We first performed analytical calculations to estimate the magnitude of the transition matrix. By rewriting the IS dipole operator in terms of the internal coordinates within clusters and the intercluster coordinate, it was shown that the transition brings about the $1\hbar\omega$ and $3\hbar\omega$ excitation to the intercluster motion. Therefore, the IS dipole transition has the potential to activate the degrees of freedom of the cluster excitation embedded in the ground state to populate the angular excited 1^- cluster states.

By assuming that the ground state is described by a shell-model wave function, we derived an analytical expression of the IS transition matrix and demonstrated that the transition matrix is indeed enhanced and is on the order of the Weisskopf estimate, even if the ground state has an ideal shell-model structure. We also performed a simple numerical calculation by using the Brink–Bloch wave function to show that the transition matrix is amplified in order of magnitude if the ground state has cluster correlation.

To provide realistic and reliable results for IS monopole and dipole transitions in ^{20}Ne and ^{44}Ti , nuclear structure calculations using Brink–Bloch GCM and AMD were performed. By taking cluster distortion into account, AMD reasonably describes the energies of those cluster states. It was shown that, despite cluster distortion, the nodal and angular excited cluster states are strongly excited by the IS monopole and dipole transitions, so we conclude that the monopole and dipole transitions are promising probes for asymmetric clustering.

ACKNOWLEDGMENTS

The authors acknowledge fruitful discussions with Dr. Kanada–En’yo, Dr. Kawabata, and Dr. Bo. Zhou, which were a great help for this work. Part of the numerical calculations were performed on the HITACHI SR16000 at KEK and YITP. This work was supported by Grants-in-Aid for Scientific Research on Innovative Areas from MEXT (Grant No. 2404:24105008) and by JSPS KAKENHI Grants No. 25400240 and No. 25800124.

APPENDIX A: ISOSCALAR DIPOLE OPERATOR REPRESENTED BY INTERNAL AND INTERCLUSTER COORDINATES

We consider the A nucleon system composed of the clusters with mass C_1 and C_2 ($C_1 + C_2 = A$) and wish to express $\mathcal{M}_\mu^{\text{IS}1}$ in terms of the internal coordinates ξ_i within each cluster and the intercluster coordinate \mathbf{r} . Noting the relations $\mathbf{R}_{C_1} - \mathbf{r}_{\text{c.m.}} = C_2/A\mathbf{r}$ and $\mathbf{R}_{C_2} - \mathbf{r}_{\text{c.m.}} = -C_1/A\mathbf{r}$, the IS dipole operator is rewritten as follows:

$$\begin{aligned}
 \mathcal{M}_\mu^{\text{IS}1} &= \sum_{i=1}^A (\mathbf{r}_i - \mathbf{r}_{\text{c.m.}})^2 \mathcal{Y}_{1\mu}(\mathbf{r}_i - \mathbf{r}_{\text{c.m.}}) \\
 &= \sum_{i \in C_1} \left(\xi_i + \frac{C_2}{A} \mathbf{r} \right)^2 \mathcal{Y}_{1\mu} \left(\xi_i + \frac{C_2}{A} \mathbf{r} \right) + \sum_{i \in C_2} \left(\xi_i - \frac{C_1}{A} \mathbf{r} \right)^2 \mathcal{Y}_{1\mu} \left(\xi_i - \frac{C_1}{A} \mathbf{r} \right) \\
 &= \sum_{i \in C_1} \xi_i^2 \mathcal{Y}_{1\mu}(\xi_i) + \sum_{i \in C_2} \xi_i^2 \mathcal{Y}_{1\mu}(\xi_i) + \left(\frac{C_2}{A} \sum_{i \in C_1} \xi_i^2 - \frac{C_1}{A} \sum_{i \in C_2} \xi_i^2 \right) \mathcal{Y}_{1\mu}(\mathbf{r}) - \frac{C_1 C_2 (C_1 - C_2)}{A^2} r^2 \mathcal{Y}_{1\mu}(\mathbf{r}) \\
 &\quad + 2 \frac{C_2}{A} \sum_{i \in C_1} (\xi_i \cdot \mathbf{r}) \mathcal{Y}_{1\mu}(\xi_i) - 2 \frac{C_1}{A} \sum_{i \in C_2} (\xi_i \cdot \mathbf{r}) \mathcal{Y}_{1\mu}(\xi_i), \tag{A1}
 \end{aligned}$$

where the relations $\sum_{i \in C_1} \xi_i = \sum_{i \in C_2} \xi_i = 0$ and $\mathcal{Y}_{1\mu}(\alpha\mathbf{a} + \beta\mathbf{b}) = \alpha\mathcal{Y}_{1\mu}(\mathbf{a}) + \beta\mathcal{Y}_{1\mu}(\mathbf{b})$ are utilized. By using the identities, $\mathbf{a} \cdot \mathbf{b} = -4\pi/\sqrt{3}[\mathcal{Y}_1(\mathbf{a}) \otimes \mathcal{Y}_1(\mathbf{b})]_{00}$, $[\mathcal{Y}_1(\mathbf{a}) \otimes \mathcal{Y}_1(\mathbf{a})]_{1\mu} = 0$, and $[\mathcal{Y}_1(\mathbf{a}) \otimes \mathcal{Y}_1(\mathbf{a})]_{2\mu} = \sqrt{3/10\pi}\mathcal{Y}_{2\mu}(\mathbf{a})$, the term in the last line

of Eq. (A1) reads

$$\begin{aligned}
(\xi_i \cdot \mathbf{r})\mathcal{Y}_{1\mu}(\xi_i) &= -\frac{4\pi}{\sqrt{3}}[\mathcal{Y}_1(\xi_i) \otimes [\mathcal{Y}_1(\xi_i) \otimes \mathcal{Y}_1(\mathbf{r})]_0]_{1\mu} \\
&= -\frac{4\pi}{\sqrt{3}} \sum_{l=0,1,2} \sqrt{2l+1} \begin{Bmatrix} 1 & 1 & l \\ 1 & 1 & 0 \end{Bmatrix} [[\mathcal{Y}_1(\xi_i) \otimes \mathcal{Y}_1(\xi_i)]_l \otimes \mathcal{Y}_1(\mathbf{r})]_{1\mu} \\
&= \frac{1}{3}\xi_i^2 \mathcal{Y}_{1\mu}(\mathbf{r}) - \sqrt{\frac{8\pi}{9}}[\mathcal{Y}_2(\xi_i) \otimes \mathcal{Y}_1(\mathbf{r})]_{1\mu}.
\end{aligned} \tag{A2}$$

We see that Eqs. (A1) and (A2) yield Eq. (12).

APPENDIX B: DERIVATION OF ISOSCALAR DIPOLE MATRIX ELEMENT

Here, we derive Eq. (13) from Eqs. (8) and (12) in a similar way as done in Ref. [31]. First, we show that the terms in Eq. (12) that involves $\mathcal{Y}_{1\mu}(\xi_i)$ and $\mathcal{Y}_{2\mu}(\xi_i)$ identically vanish in the case of the system composed of two LS closed-shell (more strictly, $SU(3)$ scalar) clusters. This is easily proved by counting the principal quantum numbers.

For example, the first term of Eq. (12) yields a matrix element proportional to

$$\left\langle \mathcal{R}_{N_{10}}(\mathbf{r}) \left(\sum_{i \in C_1} \xi_i^2 \mathcal{Y}_{10}(\xi_i) \phi_1 \right) \phi_2 \left| \mathcal{A}' \{ \mathcal{R}_{N_0 00}(\mathbf{r}) \phi_1 \phi_2 \} \right. \right\rangle.$$

Denoting the principal quantum number of ϕ_1, ϕ_2 as N_{C_1}, N_{C_2} , the principal quantum number of the ket state is equal to $N_0 + N_{C_1} + N_{C_2}$. On the other hand, that of the bra state is equal to or larger than $N + N_{C_1} + N_{C_2} + 1$, because $\sum_{i \in C_1} \xi_i^2 \mathcal{Y}_{10}(\xi_i)$ induces at least $1\hbar\omega$ excitation of ϕ_1 . Since N is equal to or larger than $N_0 + 1$, the principal quantum number of the bra state is larger than that of the ket state, so this matrix element vanishes. In the same way, the third term of the first line yields

$$\left\langle \mathcal{R}_{N_{10}}(\mathbf{r}) \mathcal{Y}_{1m}(\mathbf{r}) \left(\sum_{i \in C_1} \mathcal{Y}_{2-m}(\xi_i) \phi_1 \right) \phi_2 \left| \mathcal{A}' \{ \mathcal{R}_{N_0 00}(\mathbf{r}) \phi_1 \phi_2 \} \right. \right\rangle. \tag{B1}$$

The quantum number of $\sum_{i \in C_1} \mathcal{Y}_{2-m}(\xi_i) \phi_1$ is at least $N_{C_1} + 2$, because $\sum_{i \in C_1} \mathcal{Y}_{2-m}(\xi_i)$ generates 2^+ states of the LS closed-shell nucleus ϕ_1 which involves at least a $2\hbar\omega$ excitation. Combined with the quantum number of the intercluster motion which is at least $N - 1$, we again find that the quantum number of the bra state is larger than that of the ket state. Thus, terms that involve the internal cluster excitation vanish.

However, for the open-shell (non $SU(3)$ scalar) clusters, it must be noted that Eq. (B1) does not vanish and can be very large. A typical example is the ^{12}C cluster. For such clusters, the wave function in parentheses in Eq. (B1) is written as

$$\begin{aligned}
&\sum_{i \in ^{12}\text{C}} \mathcal{Y}_{2-m}(\xi_i) \phi_{^{12}\text{C}}(0_1^+) \\
&= \langle \phi_{^{12}\text{C}}(2_1^+) | \sum_{i \in ^{12}\text{C}} \mathcal{Y}_{2-m}(\xi_i) | \phi_{^{12}\text{C}}(0_1^+) \rangle \phi_{^{12}\text{C}}(2_1^+) \\
&\quad + \text{other excited } 2^+ \text{ states.}
\end{aligned} \tag{B2}$$

Since $\phi_{^{12}\text{C}}(2_1^+)$ has the same principal quantum number as the ground state $\phi_{^{12}\text{C}}(0_1^+)$ and the matrix element $\langle \phi_{^{12}\text{C}}(2_1^+) | \sum_{i \in ^{12}\text{C}} \mathcal{Y}_{2-m}(\xi_i) | \phi_{^{12}\text{C}}(0_1^+) \rangle$ is proportional to the large $E2$ matrix element, Eq. (B1) can be comparable or even larger than the last two terms of Eq. (12). We conclude that, if the cluster nucleus has the rotational or vibrational ground band with an enhanced $E2$ transition, the internal excitation of the cluster from 0^+ to 2^+ can have a large contribution to IS dipole excitation.

Now we evaluate the nonvanishing contribution from the last two terms of Eq. (12). The first of these terms yields the the matrix element proportional to

$$\left\langle \mathcal{R}_{N_{10}}(\mathbf{r}) \mathcal{Y}_{10}(\mathbf{r}) \left(\sum_{i \in C_1} \xi_i^2 \phi_1 \right) \phi_2 \left| \mathcal{A}' \{ \mathcal{R}_{N_0 00}(\mathbf{r}) \phi_1 \phi_2 \} \right. \right\rangle. \tag{B3}$$

Note that, in the bra state, the IS monopole operator $\sum_{i \in C_1} \xi_i^2$ induces 0 or $2\hbar\omega$ excitation of ϕ_{C_1} ,

$$\sum_{i \in C_1} \xi_i^2 \phi_1 = \langle \phi_1 | \sum_{i \in C_1} \xi_i^2 | \phi_1 \rangle \phi_1 + 2\hbar\omega \text{ excited } 0^+ \text{ states.} \tag{B4}$$

and $\mathcal{Y}_{10}(\mathbf{r})$ brings about the angular excitation of the intercluster motion with $\pm 1\hbar\omega$, i.e., the principal quantum number of the intercluster motion is equal to $N \pm 1$. Again we count the quantum numbers and find that Eq. (B3) is nonzero only when $N = N_0 + 1$, otherwise the principal quantum number of the bra state is larger than that of the ket state. From Eq. (B4) and the identities

$$\mathcal{R}_{N_{10}}(\mathbf{r}) \mathcal{Y}_{1m}(\mathbf{r}) = \sqrt{\frac{1}{4\pi}} r R_{N1}(r) Y_{00}(\hat{r}) + \sqrt{\frac{1}{5\pi}} r R_{N1}(r) Y_{20}(\hat{r}), \tag{B5}$$

$$r R_{N1}(r) = \sum_{N'} \langle R_{N'0} | r | R_{N1} \rangle R_{N'0}(r), \tag{B6}$$

Eq. (B3) is calculated as

$$\begin{aligned}
&\sqrt{\frac{1}{4\pi}} \langle \phi_1 | \sum_{i \in C_1} \xi_i^2 | \phi_1 \rangle \sum_{N'} \langle R_{N'0} | r | R_{N_0+11} \rangle \\
&\quad \times \langle R_{N'0}(r) Y_{00}(\hat{r}) \phi_1 \phi_2 | \mathcal{A}' \{ R_{N_0 00}(r) Y_{00}(\hat{r}) \phi_1 \phi_2 \} \rangle \\
&= \sqrt{\frac{1}{4\pi}} C_1 \langle r^2 \rangle_{C_1} \langle R_{N_0 0} | r | R_{N_0+11} \rangle \mu_{N_0},
\end{aligned} \tag{B7}$$

where $\langle r^2 \rangle_{C_1}$ is the square of the root-mean-square radius of ϕ_{C_1} .

Finally, the last term in Eq. (12) yields

$$\langle \mathcal{R}_{N10}(\mathbf{r})r^2\mathcal{Y}_{10}(\mathbf{r})\phi_1\phi_2 | \mathcal{A}' \{ \mathcal{R}_{N00}(\mathbf{r})\phi_1\phi_2 \} \rangle, \quad (\text{B8})$$

where $r^2\mathcal{Y}_{10}(\mathbf{r})$ brings about the nodal and angular excitations of the intercluster motion with $\pm 1\hbar\omega$ or $\pm 3\hbar\omega$, and hence the matrix element vanishes except for $N = N_0 + 1$ and $N_0 + 3$ cases. By a similar calculation, one finds that Eq. (B8) is equal to

$$\sqrt{\frac{1}{4\pi}} \langle R_{N00} | r^3 | R_{N1} \rangle \mu_{N0}, \quad (\text{B9})$$

where N is $N_0 + 1$ or $N_0 + 3$. From those results, we obtain an analytic expression for the reduced matrix element given in Eq. (13).

APPENDIX C: SIGN OF f_{N_0+1} AND f_{N_0+3}

The coefficients f_{N_0+1} and f_{N_0+3} in Eq. (4) usually have opposite sign for cluster states. To show it, we first approximate the wave function of angular excited cluster state Eq. (4) as the Brink–Bloch wave function given in Eqs. (20) and (21). This approximation may be justified because those wave functions have largely overlap each other with the proper choice of R . For example, in the case of ^{20}Ne , the overlap between the Brink–Bloch wave function with $R = 5.0$ fm and the AMD wave function for the 1_1^- state amounts to 82%.

Given that the approximation is reasonable, we substitute Eq. (22) into Eq. (21) and compare it with Eq. (4). As a result, one finds that the sign of f_N is equal to that of A_{Nl} defined by Eq. (23). Therefore, f_{N_0+1} and f_{N_0+3} should have opposite sign, if the angular excited state is well approximated by the Brink–Bloch wave function.

-
- [1] D. H. Youngblood, Y.-W. Lui, and H. L. Clark, *Phys. Rev. C* **55**, 2811 (1997).
- [2] D. H. Youngblood, Y.-W. Lui, and H. L. Clark, *Phys. Rev. C* **57**, 2748 (1998).
- [3] D. H. Youngblood, Y.-W. Lui, and H. L. Clark, *Phys. Rev. C* **60**, 014304 (1999).
- [4] Y.-W. Lui, H. L. Clark, and D. H. Youngblood, *Phys. Rev. C* **64**, 064308 (2001).
- [5] D. H. Youngblood, Y.-W. Lui, and H. L. Clark, *Phys. Rev. C* **65**, 034302 (2002).
- [6] B. John, Y. Tokimoto, Y.-W. Lui, H. L. Clark, X. Chen, and D. H. Youngblood, *Phys. Rev. C* **68**, 014305 (2003).
- [7] D. H. Youngblood, Y.-W. Lui, and H. L. Clark, *Phys. Rev. C* **76**, 027304 (2007).
- [8] T. Wakasa *et al.*, *Phys. Lett. B* **653**, 173 (2007).
- [9] T. Kawabata *et al.*, *Int. J. Mod. Phys. E* **17**, 2071 (2008).
- [10] D. H. Youngblood, Y.-W. Lui, X. F. Chen, and H. L. Clark, *Phys. Rev. C* **80**, 064318 (2009).
- [11] X. Chen, Y.-W. Lui, H. L. Clark, Y. Tokimoto, and D. H. Youngblood, *Phys. Rev. C* **80**, 014312 (2009).
- [12] M. Itoh, H. Akimune, M. Fujiwara, U. Garg, N. Hashimoto, T. Kawabata, K. Kawase, S. Kishi, T. Murakami, K. Nakanishi, Y. Nakatsugawa, B. K. Nayak, S. Okumura, H. Sakaguchi, H. Takeda, S. Terashima, M. Uchida, Y. Yasuda, M. Yosoi, and J. Zenihiro, *Phys. Rev. C* **84**, 054308 (2011).
- [13] M. R. Anders, S. Shlomo, T. Sil, D. H. Youngblood, Y.-W. Lui, and Krishichayan, *Phys. Rev. C* **87**, 024303 (2013).
- [14] Y. K. Gupta *et al.*, *Phys. Lett. B* **748**, 343 (2015).
- [15] E. Uegaki, S. Okabe, Y. Abe, and H. Tanaka, *Prog. Theor. Phys.* **57**, 1262 (1977).
- [16] E. Uegaki, Y. Abe, S. Okabe, and H. Tanaka, *Prog. Theor. Phys.* **62**, 1621 (1979).
- [17] M. Kamimura, *Nucl. Phys. A* **351**, 456 (1981).
- [18] P. Descouvemont and D. Baye, *Phys. Rev. C* **36**, 54 (1987).
- [19] Y. Kanada–En’yo, *Phys. Rev. Lett.* **81**, 5291 (1998).
- [20] A. Tohsaki, H. Horiuchi, P. Schuck, and G. Röpke, *Phys. Rev. Lett.* **87**, 192501 (2001).
- [21] Y. Funaki, A. Tohsaki, H. Horiuchi, P. Schuck, and G. Röpke, *Phys. Rev. C* **67**, 051306 (2003).
- [22] T. Neff and H. Feldmeier, *Nucl. Phys. A* **738**, 357 (2004).
- [23] Y. Funaki, A. Tohsaki, H. Horiuchi, P. Schuck, and G. Röpke, *Eur. Phys. J. A* **28**, 259 (2006).
- [24] M. Chernykh, H. Feldmeier, T. Neff, P. von Neumann-Cosel, and A. Richter, *Phys. Rev. Lett.* **98**, 032501 (2007).
- [25] Y. Suzuki and S. Hara, *Phys. Rev. C* **39**, 658 (1989).
- [26] T. Yamada, Y. Funaki, T. Myo, H. Horiuchi, K. Ikeda, G. Röpke, P. Schuck, and A. Tohsaki, *Phys. Rev. C* **85**, 034315 (2012).
- [27] Y. Suzuki, *Nucl. Phys. A* **470**, 119 (1987).
- [28] Y. Kanada–En’yo, *Phys. Rev. C* **75**, 024302 (2007).
- [29] T. Kawabata *et al.*, *Phys. Lett. B* **646**, 6 (2007).
- [30] T. Yamada and Y. Funaki, *Phys. Rev. C* **82**, 064315 (2010).
- [31] T. Yamada, Y. Funaki, H. Horiuchi, K. Ikeda, and A. Tohsaki, *Prog. Theor. Phys.* **120**, 1139 (2008).
- [32] B. F. Bayman and A. Bohr, *Nucl. Phys.* **9**, 596 (1958).
- [33] T. Ichikawa, N. Itagaki, T. Kawabata, Tz. Kokalova, and W. von Oertzen, *Phys. Rev. C* **83**, 061301 (2011).
- [34] M. Ito, *Phys. Rev. C* **83**, 044319 (2011).
- [35] M. Itoh, S. Kishi, H. Sakaguchi, H. Akimune, M. Fujiwara, U. Garg, K. Hara, H. Hashimoto, J. Hoffman, T. Kawabata, K. Kawase, T. Murakami, K. Nakanishi, B. K. Nayak, S. Terashima, M. Uchida, Y. Yasuda, and M. Yosoi, *Phys. Rev. C* **88**, 064313 (2013).
- [36] T. Kawabata *et al.*, *J. Phys.: Conf. Ser.* **436**, 012009 (2013).
- [37] Y. Kanada–En’yo, *Phys. Rev. C* **89**, 024302 (2014).
- [38] Z. H. Yang, Y. L. Ye, Z. H. Li, J. L. Lou, J. S. Wang, D. X. Jiang, Y. C. Ge, Q. T. Li, H. Hua, X. Q. Li, F. R. Xu, J. C. Pei, R. Qiao, H. B. You, H. Wang, Z. Y. Tian, K. A. Li, Y. L. Sun, H. N. Liu, J. Chen, J. Wu, J. Li, W. Jiang, C. Wen, B. Yang, Y. Y. Yang, P. Ma, J. B. Ma, S. L. Jin, J. L. Han, and J. Lee, *Phys. Rev. Lett.* **112**, 162501 (2014).
- [39] Z. H. Yang, Y. L. Ye, Z. H. Li, J. L. Lou, J. S. Wang, D. X. Jiang, Y. C. Ge, Q. T. Li, H. Hua, X. Q. Li, F. R. Xu, J. C. Pei, R. Qiao, H. B. You, H. Wang, Z. Y. Tian, K. A. Li, Y. L. Sun, H. N. Liu, J. Chen, J. Wu, J. Li, W. Jiang, C. Wen, B. Yang, Y. Liu, Y. Y. Yang, P. Ma, J. B. Ma, S. L. Jin, J. L. Han, and J. Lee, *Phys. Rev. C* **91**, 024304 (2015).
- [40] Y. Chiba and M. Kimura, *Phys. Rev. C* **91**, 061302 (2015).
- [41] H. Horiuchi and K. Ikeda, *Prog. Theor. Phys.* **40**, 277 (1968).
- [42] F. Iachello, *Phys. Lett. B* **160**, 1 (1985).

- [43] Y. Alhassid, M. Gai, and G. F. Bertsch, *Phys. Rev. Lett.* **49**, 1482 (1982).
- [44] M. Gai, M. Ruscev, A. C. Hayes, J. F. Ennis, R. Keddy, E. C. Schloemer, S. M. Sterbenz, and D. A. Bromley, *Phys. Rev. Lett.* **50**, 239 (1983).
- [45] N. Curtis, D. D. Caussyn, C. Chandler, M. W. Cooper, N. R. Fletcher, R. W. Laird, and J. Pavan, *Phys. Rev. C* **66**, 024315 (2002).
- [46] V. Z. Goldberg, K.-M. Källman, T. Lönnroth, P. Manngard, and B. B. Skorodumov, *Phys. At. Nucl.* **68**, 1079 (2005).
- [47] N. I. Ashwood *et al.*, *J. Phys. G* **32**, 463 (2006).
- [48] S. Yildiz, M. Freer, N. Soić, S. Ahmed, N. I. Ashwood, N. M. Clarke, N. Curtis, B. R. Fulton, C. J. Metelko, B. Novatski, N. A. Orr, R. Pitkin, S. Sakuta, and V. A. Ziman, *Phys. Rev. C* **73**, 034601 (2006).
- [49] H. Daley and F. Iachello, *Phys. Lett. B* **131**, 281 (1983).
- [50] M. Gai, J. F. Ennis, M. Ruscev, E. C. Schloemer, B. Shivakumar, S. M. Sterbenz, N. Tsoupas, and D. A. Bromley, *Phys. Rev. Lett.* **51**, 646 (1983).
- [51] M. Gai, J. F. Ennis, D. A. Bromley, H. Emling, F. Azgui, E. Grosse, H. J. Wollersheim, C. Mittag, and F. Riess, *Phys. Lett. B* **215**, 242 (1988).
- [52] A. Astier, P. Petkov, M.-G. Porquet, D. S. Delion, and P. Schuck, *Phys. Rev. Lett.* **104**, 042701 (2010).
- [53] Y. Suzuki and S. Ohkubo, *Phys. Rev. C* **82**, 041303 (2010).
- [54] D. S. Delion, R. J. Liotta, P. Schuck, A. Astier, and M.-G. Porquet, *Phys. Rev. C* **85**, 064306 (2012).
- [55] M. Spieker, S. Pascu, A. Zilges, and F. Iachello, *Phys. Rev. Lett.* **114**, 192504 (2015).
- [56] Y. Kanada-En'yo, [arXiv:1512.03619](https://arxiv.org/abs/1512.03619).
- [57] D. M. Brink, in *Proceedings of the International School of Physics Enrico Fermi, Course 36, Varenna*, edited by C. Bloch (Academic Press, New York, 1966).
- [58] Y. Kanada-En'yo, M. Kimura, and H. Horiuchi, *C. R. Phys.* **4**, 497 (2003).
- [59] Y. Kanada-En'yo, M. Kimura, and A. Ono, *Prog. Theor. Exp. Phys.* **2012**, 01A202 (2012).
- [60] M. Harvey and T. Sebe, *Nucl. Phys. A* **136**, 459 (1969).
- [61] T. Tomoda and A. Arima, *Nucl. Phys. A* **303**, 217 (1978).
- [62] C. Vargas, J. G. Hirsch, P. O. Hess, and J. P. Draayer, *Phys. Rev. C* **58**, 1488 (1998).
- [63] K. H. Bhatt and J. B. McGrory, *Phys. Rev. C* **3**, 2293 (1971).
- [64] J. B. McGrory, *Phys. Lett. B* **47**, 481 (1973).
- [65] A. Poves and A. Zuker, *Phys. Rep.* **70**, 235 (1981).
- [66] J. P. Elliott, *Proc. R. Soc. London, Ser. A* **245**, 562 (1958).
- [67] D. R. Tilleya, C. M. Chevesa, J. H. Kelleys, S. Ramand, and H. R. Wellera, *Nucl. Phys. A* **636**, 249 (1998).
- [68] T. Yamaya, S. Oh-ami, O. Satoh, M. Fujiwara, T. Itahashi, K. Katori, S. Kato, M. Tosaki, S. Hatori, and S. Ohkubo, *Phys. Rev. C* **41**, 2421 (1990).
- [69] T. Yamaya, K. Ishigaki, H. Ishiyama, T. Suehiro, S. Kato, M. Fujiwara, K. Katori, M. H. Tanaka, S. Kubono, V. Guimaraes, and S. Ohkubo, *Phys. Rev. C* **53**, 131 (1996).
- [70] T. Yamaya, S. Ohkubo, S. Okabe, and M. Fujiwara, *Phys. Rev. C* **47**, 2389 (1993).
- [71] I. Angelia and K. P. Marinovab, *At. Data Nucl. Data Tables* **99**, 69 (2013).
- [72] H. Horiuchi, *Prog. Theor. Phys. Suppl.* **62**, 90 (1977).
- [73] J. F. Berger, M. Girod, and D. Gogny, *Comput. Phys. Commun.* **63**, 365 (1991).
- [74] D. L. Hill and J. A. Wheeler, *Phys. Rev.* **89**, 112 (1953).
- [75] J. J. Griffin and J. A. Wheeler, *Phys. Rev.* **108**, 311 (1957).
- [76] M. Kimura, R. Yoshida, and M. Isaka, *Prog. Theor. Phys.* **127**, 287 (2012).
- [77] M. Kimura, *Phys. Rev. C* **69**, 044319 (2004).
- [78] Y. Taniguchi, M. Kimura, and H. Horiuchi, *Prog. Theor. Phys.* **112**, 475 (2004).
- [79] M. Kimura and H. Horiuchi, *Nucl. Phys. A* **767**, 58 (2006).
- [80] T. Matsuse, M. Kamimura, and Y. Fukushima, *Prog. Theor. Phys.* **53**, 706 (1975).
- [81] P.-H. Heenen, *Nucl. Phys. A* **272**, 399 (1976).
- [82] M. Kruglanski and D. Baye, *Nucl. Phys. A* **548**, 39 (1992).
- [83] B. Buck, C. B. Dover, and J.-P. Vary, *Phys. Rev. C* **11**, 1803 (1975).
- [84] Y. Fujiwara, H. Horiuchi, and R. Tamagaki, *Prog. Theor. Phys.* **62**, 122 (1979).
- [85] M. Dufour, P. Descouvemont, and D. Baye, *Phys. Rev. C* **50**, 795 (1994).
- [86] S. Takami, K. Yabana, and K. Ikeda, *Prog. Theor. Phys.* **96**, 407 (1996).
- [87] B. Zhou, Y. Funaki, H. Horiuchi, Z. Ren, G. Röpke, P. Schuck, A. Tohsaki, C. Xu, and T. Yamada, *Phys. Rev. Lett.* **110**, 262501 (2013).
- [88] E. F. Zhou, J. M. Yao, Z. P. Li, J. Meng, and P. Ring, *Phys. Lett. B* **753**, 227 (2016).
- [89] T. Yamaya, S. Oh-ami, M. Fujiwara, T. Itahashi, K. Katori, M. Tosaki, S. Kato, S. Hatori, and S. Ohkubo, *Phys. Rev. C* **42**, 1935 (1990).
- [90] J. John, C. P. Robinson, J. P. Aldridge, and R. H. Davis, *Phys. Rev.* **177**, 1755 (1969).
- [91] U. Strobusch, C. L. Fink, B. Zeidman, R. G. Markham, H. W. Fulbright, and R. N. Horoshko, *Phys. Rev. C* **9**, 965 (1974).
- [92] H. Friedrich and K. Langanke, *Nucl. Phys. A* **252**, 47 (1975).
- [93] D. Frekers, H. Eickhoff, H. Löhner, K. Poppensieker, R. Santo, and C. Wieszorek, *Z. Phys. A: At. Nucl.* (1975) **276**, 317 (1976).
- [94] D. Frekers, R. Santo, and K. Langanke, *Nucl. Phys. A* **394**, 189 (1983).
- [95] A. Chatterjee, S. Kailas, S. Saini, S. K. Gupta, and M. K. Mehta, *Z. Phys. A: At. Nucl.* (1975) **317**, 209 (1984).
- [96] F. Michel, G. Reidemeister, and S. Ohkubo, *Phys. Rev. Lett.* **57**, 1215 (1986).
- [97] T. Wada and H. Horiuchi, *Phys. Rev. C* **38**, 2063 (1988).
- [98] S. Ohkubo, Y. Hirabayashi, and T. Sakuda, *Phys. Rev. C* **57**, 2760 (1998).
- [99] F. Michel, S. Ohkubo, and G. Reidemeister, *Prog. Theor. Phys. Suppl.* **132**, 7 (1998); T. Yamaya, K. Katori, M. Fujiwara, S. Kato, and S. Ohkubo, *ibid.* **132**, 73 (1998); T. Sakuda and S. Ohkubo, *ibid.* **132**, 103 (1998).